Rh_2Mo_3N: Noncentrosymmetric *s*-wave superconductor

Wensen Wei,[1,2] G. J. Zhao,[3] D. R. Kim,[3] Chiming Jin,[1,2] J. L. Zhang,[1] Langsheng Ling,[1] Lei Zhang,[1] Haifeng Du,[1,2] T. Y. Chen,[3] Jiadong Zang,[4] Mingliang Tian,[1,2] C. L. Chien,[5] and Yuheng Zhang[1,2]

[1]*High Magnetic Field Laboratory, Chinese Academy of Sciences and University of Science and Technology of China, Hefei 230026, People's Republic of China*

[2]*Collaborative Innovation Center of Advanced Microstructures, Nanjing University, Jiangsu 210093, People's Republic of China*

[3]*Department of Physics, Arizona State University, Tempe, Arizona 85287, USA*

[4]*Department of Physics and Materials Science Program, University of New Hampshire, Durham, New Hampshire 03824, USA*

[5]*Department of Physics and Astronomy, Johns Hopkins University, Baltimore, Maryland 21218, USA*

(Received 17 April 2016; revised manuscript received 28 June 2016; published 7 September 2016)

Rh_2Mo_3N, with a noncentrosymmetric β-manganese structure, has been found to be superconducting with critical temperature $T_c \approx 4.3$ K. Magnetic field dependence of resistivity, magnetization, and specific heat measurements show that its upper critical field of $\mu_0 H_{c2}^* \sim 7.41$ T comes close to, but does not exceed, the Pauli paramagnetic limit and that the $2\Delta/k_B T_c$ value of about 3.62 is in accordance with a conventional *s*-wave superconductor. Andreev reflection spectroscopy measurements using both normal metal and half-metal show conclusively *s*-wave pairing with an isotropic gap.

DOI: 10.1103/PhysRevB.94.104503

I. INTRODUCTION

Since the discovery of the first noncentrosymmetric superconductor (SC) $CePt_3Si$ [1] with superconducting properties more complex than those within the realm of the Bardeen-Cooper-Schrieffer (BCS) theory, the role of structural asymmetry in superconductivity has attracted a great deal of attention [2–4]. The absence of inversion symmetry may result in an antisymmetric Rashba-type spin-orbit coupling (SOC), which allows mixing of the spin singlet and spin triplet Cooper pairing states, as opposed to the pure spin singlet state in most of the known SCs [5]. This aspect has motivated the search for new SCs without inversion symmetry. Better known examples of SCs without inversion symmetry include $CeRhSi_3$ [6], UIr [7], Al_2Mo_3C [8], Li_2Pt_3B [9], and others. In fact, the existence of a spin triplet state has been confirmed in Li_2Pt_3B [10], which has a perovskitelike cubic structure (space group $P4_332$) without strong electron correlation. Recently, Cr_2Re_3B, which has the β-manganese (β-Mn) structure (space group $P4_132$), has shown superconductivity at 4.8 K [11].

On the other hand, the lack of inversion symmetry also produces an antisymmetric Dzyaloshinskii-Moriya (DM) interaction [12,13]. The DM interaction, competing with the usual Heisenberg exchange interaction, plays a key role in creating noncollinear magnetic spin structures such as spin helices in the magnetic ground state and magnetic skyrmions in a narrow range of fields and temperatures, as realized in materials such as MnSi [14], FeGe [15], and Co-Zn-Mn alloy [16]. Combining the Rashba-type interaction with a DM interaction, noncentrosymmetric materials also exhibit other rich physical phenomena, such as anomalous anisotropic magnetoresistance and intrinsic resistivity of the helical state [17,18]. In contrast, the transition metal nitrides with the same β-Mn structure class show rather different physical properties contingent on the complex interactions from the broken inversion symmetry. The Ni_2Mo_3N material is paramagnetic [19], whereas $Fe_{2-x}Rh_xMo_3N$ is ferromagnetic with properties depending on the Fe content [20]. Even richer magnetic skyrmion phases are found in $Fe_xCo_{1.5-x}Rh_{0.5}Mo_3N$ ($x = 1.2, 1.0, 0.5$) [21].

In the case of Rh_2Mo_3N, it has the same β-Mn noncentrosymmetric cubic structure as schematically shown in Fig. 1(a). There are three different Wyckoff positions: an 8*c* site with Rh atoms, a 12*d* site with Mo atoms, and a 4*b* site with N atoms. The Rh atoms lie on the 8*c* positions of a cubic unit cell forming a single (10,3)-a network, while the Mo_6N octahedrons fill the space. In Rh_2Mo_3N, because of the extended 4*d* orbital of Rh, the 4*d*-4*d* hybridization between Rh and Mo orbitals becomes stronger, and the states between Rh 4*d* and Mo 4*d* orbitals become highly overlapped. At the Fermi level, the density of states (DOS) coming from Rh 4*d* of Rh_2Mo_3N is very low and cannot satisfy the Stoner criterion [22]; hence, Rh_2Mo_3N is nonmagnetic but superconducting.

In this paper, we report the synthesis of the Rh_2Mo_3N, a noncentrosymmetric SC with $T_C \sim 4.3$ K. Electrical transport, specific heat, and magnetic measurements show that, in contrast to other noncentrosymmetric materials that show unconventional superconductivity, Rh_2Mo_3N is a BCS SC. Andreev reflection spectroscopy using normal and half-metal tips confirms that it has an isotropic superconducting gap, whose temperature dependence is consistent with the BCS theory.

II. EXPERIMENT

The polycrystalline Rh_2Mo_3N sample with the β-Mn structure was synthesized by the reductive nitridation method [20]. Rh_2O_3 (99.9% pure, Alfa Aesar) and MoO_3 (99.9995% pure, Alfa Aesar) were mixed with the stoichiometric ratio and calcined in a tube furnace for 48 h at successively higher temperatures of 700 °C, 800 °C, and 850 °C under a flowing atmosphere of a gas mixture of 10% H_2 + 90% N_2. After each temperature, the calcined powder sample was thoroughly reground. X-ray diffraction (XRD) was used to verify its crystal structure. The dc magnetization and resistivity measurements were carried out by a Magnetic Property Measurement System (MPMS) and Physical Property Measurement System (PPMS) from Quantum Design. The Andreev reflection spectroscopy (ARS) was further employed to determine the superconducting gap and spin configuration of the Cooper pairs.

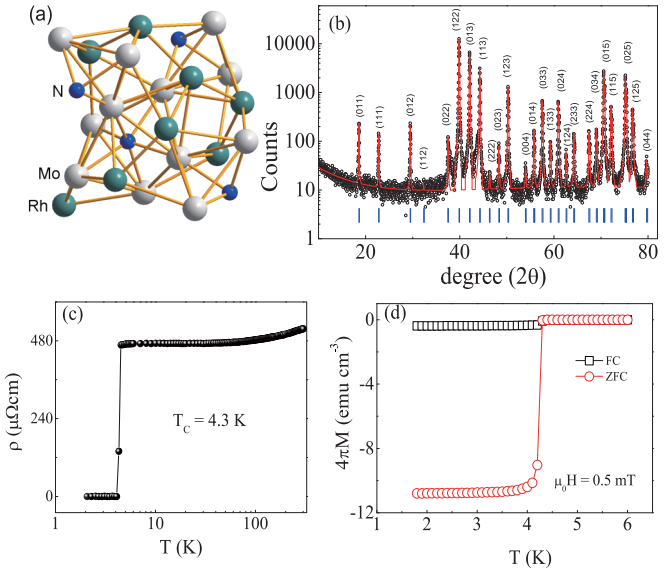

FIG. 1. (a) Crystal structure of Rh_2Mo_3N. Sketch of crystal with β-Mn structure with Rh atoms at the 8c position of a unit cell forming a single (10,3)-a network, and the Mo_6N octahedrons filling in the space. (b) Observed (open circles) and calculated (red line) x-ray diffraction patterns of Rh_2Mo_3N. Some are labeled with Miller indices. The tick marks indicate all the diffraction peaks. (c, d) Superconducting phenomena of Rh_2Mo_3N. Temperature dependence of (c) resistivity and (d) magnetization both show superconducting transition at 4.3 K from (c) resistivity and (d) diamagnetic phenomena.

III. RESULT AND DISCUSSION

As shown in Fig. 1(b), the XRD spectrum confirms that our sample has a cubic noncentrosymmetric structure with $a = b = c = 6.81$ Å and a space group $P4_132$ by the Rietveld refinement method. The tick marks indicate the allowed positions for diffraction, indicating the sample is polycrystalline. The extracted structure parameters are listed in Table I. Figures 1(c) and 1(d) show the resistivity and magnetization, respectively, as functions of temperature. The resistivity shows a sharp drop to zero at 4.3 K, accompanied by diamagnetic behavior with T_c also at 4.3 K. To gain further information concerning its superconducting properties, magnetization and resistivity as functions of magnetic field were measured at various temperatures, as shown in Figs. 2(a) and 2(e). Figure 2(b) shows the M-H loop at 2 K, indicating that Rh_2Mo_3N is a type II SC, and the superconducting volume fraction calculated from the magnetic measurement exceeds 100%, which comes from the demagnetization field due to irregular shapes of the grains. The bulk superconductivity can be confirmed by the specific heat measurement, as shown below.

TABLE I. Crystal structure parameters of Rh_2Mo_3N. The data were obtained by using the Rietveld method with x-ray diffraction data. Its space group is $P4_132$, and its crystal constant is $a = b = c = 6.8124(0)$ Å.

Atom	x	y	z	U_{iso}/Å^2
Rh	0.06343(3)	0.06343(3)	0.06343(3)	0.01185
Mo(12d)	0.125	0.20438(5)	0.45438(5)	0.00701
N(4b)	0.375	0.375	0.375	0.01322

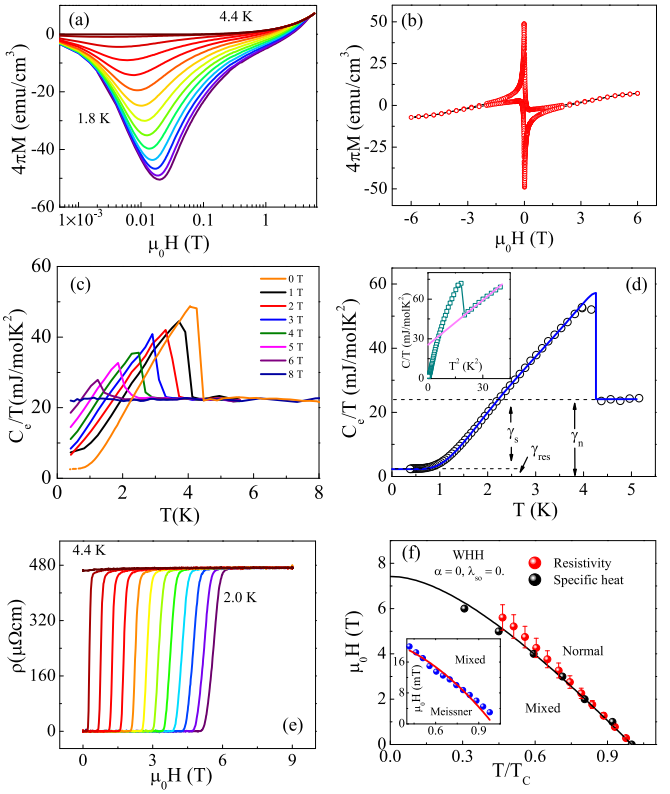

FIG. 2. (a) Magnetization versus magnetic field curves at temperatures varying from 1.8 to 4.4 K of Rh_2Mo_3N powder. (b) The M-H loop of Rh_2Mo_3N powder up to 6 T at 2 K. (c) In order to subtract the heat capacity background, C_e/T versus T at various applied fields were calculated. (d) The electronic contribution of specific heat from the experiment was fit by using the BCS theory; (inset) the total C/T versus T^2 at zero field with the $C(T,H)/T = \gamma_n + \beta_1 T^2$ fitting (magenta solid line). (e) The field dependence of electrical resistivity at temperatures varying from 2.0 to 4.4 K of a small Rh_2Mo_3N tablet. (f) The upper critical field versus T/T_c of the Rh_2Mo_3N inferred from the electrical and specific heat measurements. The data was fit by using the WHH model; (inset): the lower critical field determined from the magnetic measurement versus T/T_c and its fitting (see text).

The phase diagram of H_{c2} versus T/T_c is shown in Fig. 2(f). The lower critical field $H_{c1}(T)$ shown in the inset of Fig. 2(f) is determined from the M-H curves in Fig. 2(a), where $H_{c1}(T)$ was defined from the point deviating from the linear curve due to the Meissner effect. A fit using the well-known formula $H_{c1}(T) = H_{c1}(0)\{1 - (\frac{T}{T_c})^2\}$ yields $\mu_0 H_{c1}(0) = 23.0$ mT, a value similar to those of most BCS-like SCs such as superconducting Pb-In alloys [23], $PbTaSe_2$ [24], Re_7B_3 [25], and so on. The London penetration depth of $\lambda(0) = 169.22$ nm has been calculated using $\mu_0 H_{c1}(0) \approx \Phi_0/\pi\lambda(0)^2$, where μ_0 is the vacuum permeability, and $\Phi_0 = 2.07 \times 10^{-15}$ Wb is the flux quantum. The upper critical field, $H_{c2}(T)$, was defined from the midpoint of the resistivity drop at which the applied magnetic field drives the sample to the normal state [Fig. 2(e)]. Furthermore, the upper critical field can also be determined from the specific heat measurement under an applied field,

as shown in Fig. 2(c). The obtained values are close to the results from the resistivity method, as shown in Fig. 2(f). We use the Werthamer-Helfand-Hohenberg (WHH) model [26] to fit the H_{c2} vs. T/T_c curve by considering orbital breaking, including the effect of Pauli spin paramagnetism and spin-orbit scattering, which are described by two parameters, α and λ_{so}, respectively. The value of α allows a rough discrimination between the Pauli limit and orbital pair breaking, while λ_{so} is dominated by the atomic numbers of the elements of the material under consideration. In the WHH model,

$$\ln\frac{1}{t} = \left(\frac{1}{2}+\frac{i\lambda_{so}}{4\gamma}\right)\psi\left(\frac{1}{2}+\frac{\bar{h}+\frac{\lambda_{so}}{2}+i\gamma}{2t}\right)+\left(\frac{1}{2}-\frac{i\lambda_{so}}{4\gamma}\right)\times\psi\left(\frac{1}{2}+\frac{\bar{h}+\frac{\lambda_{so}}{2}-i\gamma}{2t}\right)-\psi\left(\frac{1}{2}\right) \quad (1)$$

where $t = T/T_c$, $\gamma \equiv [(\alpha\bar{h})^2 - (\lambda_{so}/2)^2]^{1/2}$, ψ is the digamma function, and

$$h^* \equiv \frac{\bar{h}}{\left(-\frac{d\bar{h}}{dt}\right)_{t=1}} = \frac{\pi^2\bar{h}}{4} = \frac{H_{c2}}{\left(-\frac{H_{c2}}{dt}\right)_{t=1}} \quad (2)$$

The data obtained from the heat capacity measurements fit well to the WHH model, while the data obtained from the resistivity measurements show a slight deviation. A similar phenomenon has also been observed in $BaPtSi_3$ [27]. Additionally, the fitting parameters $\alpha = 0, \lambda_{so} = 0$, indicate negligible roles of the spin-paramagnetic effect and the spin-orbit interaction played in this material. As a consequence, Rh_2Mo_3N is capable of reaching a very high upper critical field. In this case ($\alpha = 0$, $\lambda_{so} = 0$), the upper critical field at 0 K follows the relation

$$\mu_0 H^*_{c2}(0) = -0.693\left(\frac{d\mu_0 H_{c2}}{dT}\right)_{T_c} T_c \quad (3)$$

From this relation we obtain $\mu_0 H^*_{c2}(0) = 7.41\ T$, which is close to, but still below, the Pauli paramagnetic limit of $\mu_0 H_P = \frac{\Delta}{\sqrt{2}\mu_B} \approx 7.87$ T, where 2Δ is the superconducting gap energy. The value indicates that orbital breaking is the main mechanism that limits the upper critical field. The lack of inversion symmetry, although favoring a higher critical field, fails to exceed, but comes tantalizingly close to, the Pauli paramagnetic limit. Therefore, Rh_2Mo_3N remains a conventional BCS-like SC notwithstanding the inversion symmetry breaking in the crystal structure. The coherence length of $\xi_o = 6.67$ nm can be obtained from the relation $\mu_0 H_{c2}(0) \approx \Phi_0/(2\pi\xi(0)^2)$. From the London penetration depth and the coherence length, the Ginzburg-Landau parameter is $\kappa_{GL} = \frac{\lambda}{\xi} \approx 25.37$, which again confirms that Rh_2Mo_3N is a type II SC.

Figure 2(c) shows the specific heat measurements under different magnetic fields. A clear jump near T_c indicates a second-order phase transition with a bulk nature. When applying a magnetic field, the jump gradually diminishes and shifts towards low temperature. When the field is up to 8.0 T, superconductivity is completely suppressed without any specific heat anomaly [Fig. 2(c)]. The total specific heat consists of both electronic and phonon contributions; that is, $C(T,H) = \gamma_n T + \beta_1 T^3$. The first term is the electronic component, while the latter denotes the phonon contribution. The inset of Fig. 2(d) shows the fit to $C(T,H) = \gamma_n T + \beta_1 T^3$. It yields the Sommerfeld coefficient $\gamma_n = 24.15\ \mathrm{mJ\,mol^{-1}\,K^{-2}}$, and $\beta_1 = 1.13\ \mathrm{mJ\,mol^{-1}\,K^{-4}}$. Hence, the Debye temperature $\Theta_D \sim 218$ K is derived by the formula $\beta_1 = N\pi^4 R\Theta_D^{-3}\,12/5$, where $R = 8.314\ \mathrm{J\,mol^{-1}\,K^{-1}}$, and $N = 6$. To obtain electronic specific heat C_e, two methods are employed since the electronic part is field dependent, while the phonon one is field independent in the total $C(T,H)$. Thus the field measurement can be used to subtract a heat capacity background coming from the lattice and the normal state electronic contributions. The first method is to directly subtract the phonon contribution from the total heat capacity by $C_e = C(T,H) - C_{ph} = C(T,H) - \beta_1 T^3$. The second one is using the reference value at $\mu_0 H = 8$ T where superconductivity is completely suppressed, i.e. $C_e = C(T, \mu_0 H = 0\,\mathrm{T}) - (T, \mu_0 H = 8\,\mathrm{T}) + \gamma_n T$. Indeed, both methods give almost the same result. The resulting electronic heat capacity [shown in Fig. 2(d)] fits well with the BCS theory. The fit is very good with the gap ratio $\Delta(0) = 1.81 k_B T_c$, or $2\Delta(0)/k_B T_c = 3.62$, which is quite close to the 3.52 predicted by the BCS theory. These results all indicate Rh_2Mo_3N to be a weak coupling s-wave superconductor. Note that there exists a small residual γ_{res}, leading to a nonzero electronic specific heat at the 0 K limit. This phenomenon is observed in the $Cu_xBi_2Se_3$ [28] and Ru_7B_3 [25] as well. This might come from the inevitable presence of impurities, although XRD suggests the high quality of our samples. The value of the γ_{res} is about $2.3\ \mathrm{mJ\,mol^{-1}\,K^{-2}}$, small enough when comparing to γ_n; the ratio of $\gamma_s/\gamma_n = (\gamma_n - \gamma_{res})/\gamma_n \sim 90\%$, supporting the quite high quality of the sample.

To investigate the pairing state of the superconductivity in Rh_2Mo_3N, we utilize ARS to determine the superconducting gap and the spin configuration of the Cooper pairs. Electrons must form Cooper pairs in the superconducting state, so a single electron cannot be injected from a normal metal (N) into a SC, unless it is accompanied by another electron with the proper spin direction by reflecting a hole back into the normal metal. This is the celebrated Andreev reflection process [29]. The availability of the other electron with the proper spin imposes a limit on the conductance of the N/SC interface for injection energy within the superconducting gap. This feature can also be used to measure the spin polarization (P) of any metal, defined as the difference of spin-up and spin-down electrons at the Fermi level, $P \equiv \frac{N_\uparrow(E_F) - N_\downarrow(E_F)}{N_\uparrow(E_F) + N_\downarrow(E_F)}$, where $N_\uparrow(E_F)$ and $N_\downarrow(E_F)$ are densities of electrons with spin-up and spin-down, respectively, at the Fermi energy E_F. The conductance across the N/SC interface is normalized to 1 for electrons with energy (E) larger than the SC gap (Δ). A nonmagnetic metal has equal spin-up and spin-down electrons at E_F ($P = 0$), so an injected electron within the gap ($E < \Delta$) can always find another electron to go into the SC and form a Cooper pair; thus, the conductance is 2. For a half-metal ($P = 1$) where there is only one spin band available at E_F, the conductance within the gap now depends heavily on the spin configuration of the Cooper pairs in the SC. For a singlet SC, the two electrons in a Cooper pair must be antiparallel; hence, the conductance within the gap ($E < \Delta$) is 0 because there is no electron of opposite spin available to form a Cooper pair.

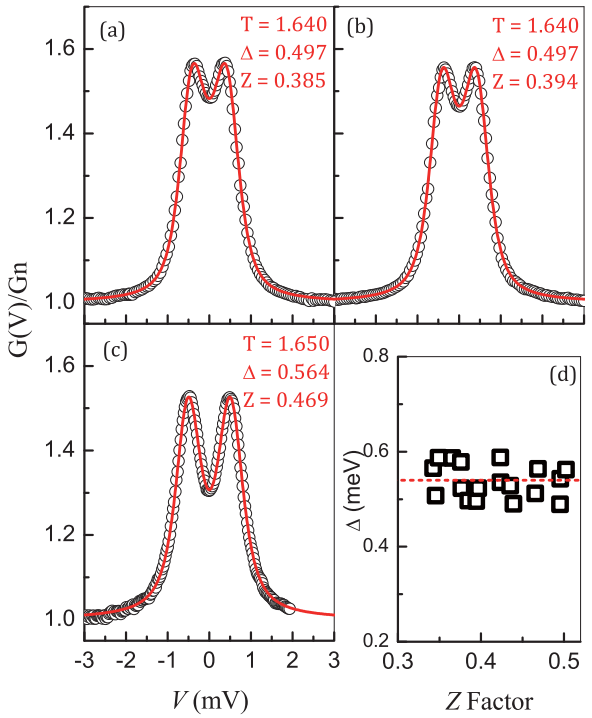

FIG. 3. Andreev reflection spectroscopy of a gold tip in contact with Rh_2Mo_3N. (a–c) Representative Andreev spectra of various Z factors and their best fits to the modified BTK model, where open circles are the experimental data and the red curves are the BTK model; (d) determined gap value of various contacts with different Z factors, with dashed line at $\Delta = 0.54 \pm 0.04$ meV.

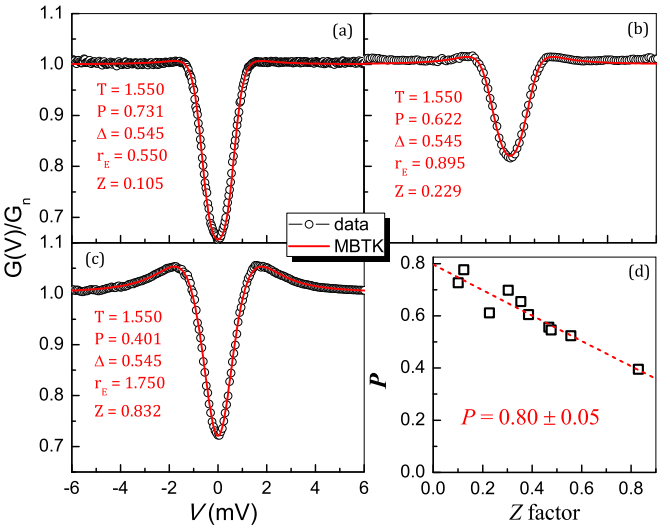

FIG. 4. Andreev reflection spectroscopy of a LSMO tip in contact with Rh_2Mo_3N. (a–c) Representative Andreev spectra with various Z factors and their best fits to the modified BTK model; (d) determined spin polarization of LSMO as a function of the Z factor and the intrinsic spin polarization of LSMO.

For a triplet SC, the spins in the Cooper pair have parallel spins so the conductance ($E < \Delta$) can also be 2. Thus, ARS provides a decisive signature to differentiate the singlet and triplet SCs. ARS has also been utilized to determine the superconducting gap of many SCs, including the conventional SCs, two band gap MgB_2 [30], Fe-SCs [31,32], and triplet SCs [33,34]. In addition, using an s-wave singlet SC with an isotropic gap, ARS has been utilized to determine the spin polarization of many magnetic materials, including common magnetic metals [35–39], highly spin-polarized materials [40], and half-metals with $P = 1$ [41,42].

Here, we first use a gold tip to determine the superconducting gap of the Rh_2Mo_3N SC. A gold tip is chosen because it is unpolarized and does not oxidize. The gold tip is made by breaking an 8-mil gold wire; it has been shown that a sharp tip with a few atoms can be formed with this method [43]. The sample was cut to have a fresh surface just before the sample and the gold tip were mounted into a vacuum jacket. The sample was then cooled down to 4.2 K in a sample tube, and 1.5 K is realized by pumping the sample tube. The point contacts are established after the temperature has been stabilized. Subsequently, the conductance (I/V) and differential conductance (dI/dV) are measured simultaneously.

Over 20 conductance spectra were measured, and some representative curves at about 1.6 K are shown in Figs. 3(a)–3(c). The open circles are the experimental data, and the solid lines are best fits to the modified Blonder-Tinkham-Klapwijk (BTK) model [44–48]. In the fitting, we use the experimental temperature and the P value of gold as 0 but vary gap Δ and a parameter, the interfacial scattering factor Z, in the BTK model. The data can be well described by the model, and the Z factors of most spectra are between 0.3 and 0.5. The gap values of all the contacts are close to 0.54 meV, as shown in Fig. 3(d). One notes that the sample is polycrystalline and the contacts are random on the sample. Different contacts essentially contact on different crystalline directions of the sample. A constant gap value for all contacts is a telltale indication that the gap is isotropic. The averaged gap value of Rh_2Mo_3N SC is $\Delta = 0.54 \pm 0.04$ meV.

Next, we use a half-metal, $La_{2/3}Sr_{1/3}MnO_3$ (LSMO), to measure the spin configuration of the Cooper pairs in the Rh_2Mo_3N SC at 1.55 K. The single-crystal LSMO was polished into a sharp tip and follows the same procedure as that of the gold tip. We have measured over 10 different contacts with various Z factors. Some representative Andreev spectra are shown in Figs. 4(a)–4(c). Again, open circles are the experimental data and solid curves are the best fits to the modified BTK (MBTK) model. The double Andreev peaks are often an indication of the gap of the SC, but the two peaks in Fig. 5(c) are nearly 2 meV, much larger than the 0.54 meV value determined by the gold tip. This is due to the much larger resistivity of the LSMO tip. Because of the large resistivity of LSMO, an extra resistance (r_E) is present in the ARS; the effects of r_E have been discussed previously by others [45,46]. With the effect of r_E included in the analysis, the determined gap value is still around 0.54 meV for all the contacts. Since we have determined the gap value using a gold tip above, in the fitting, the gap value is fixed at 0.54 meV and the temperature is fixed at experimental values; only the Z factor, P, and r_E are varied in analysis. The measured P values of all the contacts are plotted in Fig. 4(d) as function of the Z factor. The P value decreases for increasing Z factor due to the spin-flip scattering at the interface. The intrinsic

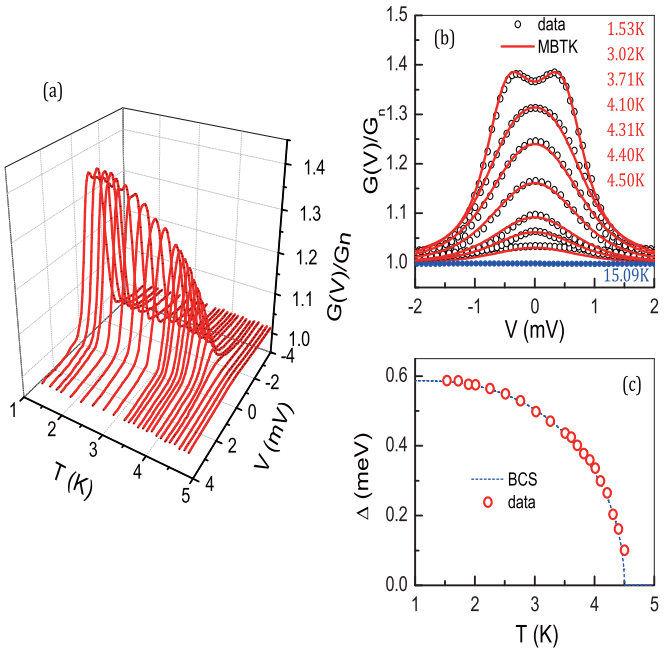

FIG. 5. Temperature dependence of Andreev reflection spectroscopy of a gold tip in contact with Rh_2Mo_3N. (a) Andreev reflection from 1.5 to 5 K, (b) best fits of Andreev spectra at various temperatures to the modified BTK model, and (c) the determined gap Δ as a function of temperature; the dashed line is from the BCS theory to guide one's eye.

P value of the LSMO is obtained by extrapolating the Z factor to 0, which is about 80%, consistent with previous studies [49]. Because the Andreev reflection is allowed for a half-metallic current using a triplet SC with parallel spin pairing, the P value of LSMO should be an apparent value of 0, the same as that of Au, if the Rh_2Mo_3N is purely spin triplet. Therefore, it conclusively shows that the spins of the Cooper pairs in the Rh_2Mo_3N SC must be antiparallel instead, as in singlet SCs.

We further measure the temperature dependence of the Andreev spectra using a gold tip. As shown in Fig. 5(a), for increasing T, the separation of the double Andreev peaks decreases gradually to become a single peak of decreasing amplitude, finally to about 1 around 4.5 K. The data at various temperatures can be well described by the modified BTK model, and some representative Andreev spectra are shown in Fig. 5(b), with open circles as the data and solid curves as the best fits to the modified BTK model [46]. In the fitting, the Z factor and the inelastic factor Γ are fixed at $Z = 0.35$, $\Gamma = 0.13$, and $r_E = 0.0$, which have been determined by the Andreev spectrum at the lowest temperature $T = 1.53$ K. Since the spectra are all from the same contact, these parameters should not change at the low temperature range. Only the gap value is varied for different T. The obtained gap value as a function of T is shown in Fig. 5(d). The dashed line is the BCS theory, using 4.5 K as T_C. One can see that the temperature dependence of the gap is very consistent with an s-wave SC of BCS theory. Interestingly, the Andreev spectra do not immediately reduce to a flat spectrum of 1 at $T > 4.5$ K. As shown in Fig. 5(b), at 4.5K, about 5% of Andreev intensity still exists, which gradually decreases to 1 at 15 K, as shown by the blue curve in Fig. 5(b). We have observed the effects for a few other contacts with temperature dependence. While this requires further study with better quality samples, such as single crystals, it might be because the point contact is very small and a small force from a tip can have a large pressure at the contact region.

The nearly consistent gap value of $2\Delta \approx 1.1$ meV, directly observed from ARS and deduced from specific heat, shows that the dominant electron pairings in Rh_2Mo_3N are singlet s-waves. Using both unpolarized (Au) and polarized (LSMO) metals, ARS indicates no triplet parallel spin configuration in the Rh_2Mo_3N SC. Combined with the specific heat and critical field results, the dominant pairings in the Rh_2Mo_3N SC are singlets with an isotropic s-wave gap.

The nature of superconductivity depends on the symmetry of the crystal structure. The inversion symmetry leads to the pure triplet or singlet pairings, while the latter is energetically preferred by time reversal symmetry. Finding a triplet SC is an extremely difficult problem. However, in noncentrosymmetric SCs, the spatial part of the electron wave functions are not necessarily symmetric or antisymmetric. To preserve the overall antisymmetry of the wave function in exchanging the two electrons, the Cooper pairs in these systems are often a mixture of spin singlet and spin triplet states [5]. The ratio between the triplet and the singlet portions depends on the SOC of the material, or more precisely speaking, the antisymmetric SOC (ASOC) strength [5]. In general, the SOC lifts degeneracies of the electron band structure at high-symmetry points. This happens to not only noncentrosymmetric materials but also centrosymmetric structures. However, the ASOC that only survives on the noncentrosymmetric materials plays a pivotal role in the spin-triplet-dominant noncentrosymmetric SCs, since it lifts the double spin degeneracy of the bands [50]. The strength of ASOC largely relies on the distortion of the crystal structure [51]. Hence in noncentrosymmetric SCs, the more dramatically the crystal structure deforms, the stronger the ASOC and, in consequence, the band splitting, will be. As a result, the spin triplet component gets more chance to dominate the Cooper pairs of the SC. For example, in $CePt_3Si$, UIr, and Li_2Pt_3B, both SOC and ASOC are fairly strong [2–4]; thus, the triplet pairing is dominant. In contrast, in our Rh-based SC with noncentrosymmetric β-Mn structures, even though the spin-orbital coupling is already significant, as evidenced by the presence of skyrmions in magnetically doped samples [21], the pairing is still singlet. This experiment suggests the ultrasensitivity of triplet SC on spin-orbital coupling. From the ARS experiment data, we cannot exclude the antiparallel component of the spin triplet state, but unequivocally there is a negligible parallel component in this material. The absence of a parallel spin triplet component is mainly due to the weak ASOC in this material. In contrast, the spin triplet SC $Li_2(Pd_{1-x}Pt_x)_3B$, although it owns the same point group as Rh_2Mo_3N, significantly distorts its crystal when platinum is doped into the $B(Pd,Pt)_6$ octahedral units [51]. As the noncentrosymmetry in Rh_2Mo_3N comes from the Mo_6N octahedral and the Rh single (10,3)-a network, we expect that partial substitution of Rh or Mo by other heavy elements can lead to large structural distortion and promising spin triplet SCs. Fortunately, doping heavy elements like platinum or palladium and magnetic elements like cobalt

or iron in Rh_2Mo_3N have been proved feasible, and the β-Mn structure persists robustly [21,52,53].

Interestingly, when Rh_2Mo_3N is doped by both cobalt and iron simultaneously, chiral magnetism is induced, and the helical spin ground state is emergent. When a small magnetic field is turn on, the magnetic skyrmion and its lattice have been observed [21]. This observation not only indicates the intimate relation between chiral magnets and noncentrosymmetric superconductors, it also suggests that this Rh_2Mo_3N system is an ideal platform for studying the complex interplay between the SCs and the spin helix or skyrmions.

IV. SUMMARY

In summary, we have synthesized a polycrystalline sample Rh_2Mo_3N with a noncentrosymmetric β-Mn structure. From the transport, specific heat, magnetic, and ARS measurements, Rh_2Mo_3N behaves as a typical BCS type II superconductor with transition temperature $T_C \sim 4.3$ K. It indicates no spin triplet pairing features from the upper critical field specific heat and ARS measurements. Although the spin triplet pairing state or mixture is theoretically allowed in a superconductor with noncentrosymmetric structure, the breaking of inversion symmetry is nonconsequential on superconductivity in Rh_2Mo_3N, which shows only s-wave singlet superconductivity.

ACKNOWLEDGMENTS

Work at Arizona State University and Johns Hopkins University was supported as part of Spins and Heat in Nanoscale Electronic Systems (SHINES), an Energy Frontier Research Center (EFRC) funded by the US Department of Energy (DOE) Basic Energy Science under Award No. SC0012670. Work at High Magnetic Field Laboratory in Hefei, People's Republic of China, was supported by Natural Science Foundation of China (NSFC), Grants No.11474290, No. 11374302, No. U1432251, No. U1332209, and No. 11504378; the Youth Innovation Promotion Association CAS No. 2015267; and the Chinese Academy of Sciences/State Administration of Foreign Experts Affairs (CAS/SAFEA) international partnership program for creative research teams of China.

[1] E. Bauer, G. Hilscher, H. Michor, C. Paul, E. W. Scheidt, A. Gribanov, Y. Seropegin, H. Noël, M. Sigrist, and P. Rogl, Phys. Rev. Lett. **92**, 027003 (2004).
[2] E. Bauer and M. Sigrist, *Non-centrosymmetric Superconductors: Introduction and Overview* (Springer, Berlin, 2012).
[3] S. Yip, Annu. Rev. Condens. Mater. Phys. **5**, 15 (2014).
[4] F. Kneidinger, E. Bauer, I. Zeiringer, P. Rogl, C. Blass-Schenner, D. Reith, and R. Podloucky, Physica C **514**, 388 (2015).
[5] L. P. Gor'kov and E. I. Rashba, Phys. Rev. Lett. **87**, 037004 (2001).
[6] N. Kimura, K. Ito, K. Saitoh, Y. Umeda, H. Aoki, and T. Terashima, Phys. Rev. Lett. **95**, 247004 (2005).
[7] T. Akazawa, H. Hidaka, T. Fujiwara, T. C. Kobayashi, E. Yamamoto, Y. Haga, R. Settai, and Y. Nuki, J. Phys.: Condens. Matter. **16**, L29 (2004).
[8] A. B. Karki, Y. M. Xiong, I. Vekhter, D. Browne, P. W. Adams, D. P. Young, K. R. Thomas, J. Y. Chan, H. Kim, and R. Prozorov, Phys. Rev. B **82**, 064512 (2010).
[9] P. Badica, T. Kondo, and K. Togano, J. Phys. Soc. Jpn. **74**, 1014 (2005).
[10] M. Nishiyama, Y. Inada, and G.-q. Zheng, Phys. Rev. Lett. **98**, 047002 (2007).
[11] H. Niimura, K. Kawashima, K. Inoue, M. Yoshikawa, and J. Akimitsu, J. Phys. Soc. Jpn. **83**, 044702 (2014).
[12] I. Dzyaloshinsky, J. Phys. Chem. Solids **4**, 241 (1958).
[13] T. Moriya, Phys. Rev. **120**, 91 (1960).
[14] S. Mühlbauer, B. Binz, F. Jonietz, C. Pfleiderer, A. Rosch, A. Neubauer, R. Georgii, and P. Böni, Science **323**, 915 (2009).
[15] X. Z. Yu, N. Kanazawa, Y. Onose, K. Kimoto, W. Z. Zhang, S. Ishiwata, Y. Matsui, and Y. Tokura, Nature Mater. **10**, 106 (2011).
[16] Y. Tokunaga, X. Z. Yu, J. S. White, H. M. Rønnow, D. Morikawa, Y. Taguchi, and Y. Tokura, Nature Commun. **6**, 7638 (2015).
[17] S. X. Huang, F. Chen, J. Kang, J. Zang, G. J. Shu, F. C. Chou, and C. L. Chien, arXiv:1409.7867.
[18] S. X. Huang, F. Chen, J. Kang, J. Zang, G. J. Shu, F. C. Chou, and C. L. Chien, New J. Phys. **18**, 065010 (2016).
[19] T. J. Prior and P. D. Battle, J. Solid State Chem. **172**, 138 (2003).
[20] S. E. Oldham, P. D. Battle, S. J. Blundell, M. L. Brooks, F. L. Pratt, and T. J. Prior, J. Mater. Chem. **15**, 3402 (2005).
[21] W. Li, C. Jin, R. Che, W. Wei, L. Lin, L. Zhang, H. Du, M. Tian, and J. Zang, Phys. Rev. B **93**, 060409(R) (2016).
[22] D. J. Singh, Phys. Rev. B **78**, 094511 (2008).
[23] J. D. Livingston, J. Appl. Phys. **34**, 3028 (1963).
[24] G. M. Pang, M. Smidman, L. X. Zhao, Y. F. Wang, Z. F. Weng, L. Q. Che, Y. Chen, X. Lu, G. F. Chen, and H. Q. Yuan, Phys. Rev. B **93**, 060506(R) (2016).
[25] Lei Fang, Huan Yang, Xiyu Zhu, Gang Mu, Zhao-Sheng Wang, Lei Shan, Cong Ren, and Hai-Hu Wen, Phys. Rev. B **79**, 144509 (2009).
[26] N. R. Werthamer, E. Helfand, and P. C. Hohenberg, Phys. Rev. **147**, 295 (1966).
[27] E. Bauer, R. T. Khan, H. Michor, and E. Royanian, Phys. Rev. B **80**, 064504 (2009).
[28] M. Kriener, Kouji Segawa, Zhi Ren, Satoshi Sasaki, and Yoichi Ando, Phys. Rev. Lett. **106**, 127004 (2011).
[29] A. F. Andreev, Zh. Éksp. Teor. Fiz. **46**, 1823 (1964) [Sov. Phys. JETP **19**, 1228 (1964)].
[30] P. Szabó, P. Samuely, J. Kačmarčík, T. Klein, J. Marcus, D. Fruchart, S. Miraglia, C. Marcenat, and A. G. M. Jansen, Phys. Rev. Lett. **87**, 137005 (2001).
[31] T. Y. Chen, Z. Tesanovic, R. H. Liu, X. H. Chen, and C. L. Chien, Nature (London) **453**, 1224 (2008).
[32] P. Szabó, Z. Pribulová, G. Pristáš, S. L. Bud'ko, P. C. Canfield, and P. Samuely, Phys. Rev. B **79**, 012503 (2009).
[33] F. Laube, G. Goll, H. v. Löhneysen, M. Fogelström, and F. Lichtenberg, Phys. Rev. Lett. **84**, 1595 (2000).

[34] X.-X. Gong, H.-X. Zhou, P.-C. Xu, D. Yue, K. Zhu, X.-F. Jin, H. Tian, G.-J. Zhao, and T.-Y. Chen, Chin. Phys. Lett. **32**, 067402 (2015).
[35] S. K. Upadhyay, A. Palanisami, R. N. Louie, and R. A. Buhrman, Phys. Rev. Lett. **81**, 3247 (1998).
[36] R. J. Soulen, Jr., J. M. Byers, M. S. Osofsky, B. Nadgorny, T. Ambrose, S. F. Cheng, P. R. Broussard, C. T. Tanaka, J. Nowak, J. S. Moodera, A. Barry, and J. M. D. Coey, Science **282**, 85 (1998).
[37] G. J. Strijkers, Y. Ji, F. Y. Yang, C. L. Chien, and J. M. Byers, Phys. Rev. B **63**, 104510 (2001).
[38] T. Y. Chen, C. L. Chien, and C. Petrovic, Appl. Phys. Lett. **91**, 142505 (2007).
[39] S. X. Huang, T. Y. Chen, and C. L. Chien, Appl. Phys. Lett. **92**, 242509 (2008).
[40] L. Wang, K. Umemoto, R. M. Wentzcovitch, T. Y. Chen, C. L. Chien, J. G. Checkelsky, J. C. Eckert, E. D. Dahlberg, and C. Leighton, Phys. Rev. Lett. **94**, 056602 (2005).
[41] Y. Ji, G. J. Strijkers, F. Y. Yang, C. L. Chien, J. M. Byers, A. Anguelouch, G. Xiao, and A. Gupta, Phys. Rev. Lett. **86**, 5585 (2001).
[42] J. S. Parker, S. M. Watts, P. G. Ivanov, and P. Xiong, Phys. Rev. Lett. **88**, 196601 (2002).
[43] H. Ohnishi, Y. Kondo, and K. Takayanagi, Nature **395**, 780 (1998).
[44] G. E. Blonder, M. Tinkham, and T. M. Klapwijk, Phys. Rev. B **25**, 4515 (1982).
[45] T. Y. Chen, Z. Tesanovic, and C. L. Chien, Phys. Rev. Lett. **109**, 146602 (2012).
[46] T. Y. Chen, S. X. Huang, and C. L. Chien, Phys. Rev. B **81**, 214444 (2010).
[47] P. Chalsani, S. K. Upadhyay, O. Ozatay, and R. A. Buhrman, Phys. Rev. B **75**, 094417 (2007).
[48] G. T. Woods, R. J. Soulen, Jr., I. I. Mazin, B. Nadgorny, M. S. Osofsky, J. Sanders, H. Srikanth, W. F. Egelhoff, and R. Datla, Phys. Rev. B **70**, 054416 (2004).
[49] Y. Ji, C. L. Chien, Y. Tomioka, and Y. Tokura, Phys. Rev. B **66**, 012410 (2002).
[50] F. Kneidinger, L. Salamakha, E. Bauer, I. Zeiringer, P. Rogl, C. Blaas-Schenner, D. Reith, and R. Podloucky, Phys. Rev. B **90**, 024504 (2014).
[51] S. Harada, J. J. Zhou, Y. G. Yao, Y. Inada, and Guo-qing Zheng, Phys. Rev. B **86**, 220502(R) (2012).
[52] T. J. Prior, S. E. Oldham, V. J. Couper, and P. D. Battle, Chem. Mater. **17**, 1867 (2005).
[53] P. D. Battle, F. Grandjean, G. J. Longc, and S. E. Oldham, J. Mater. Chem. **17**, 4785 (2007).